



Dual Leucine Zipper Kinase Regulates Dscam Expression through a Noncanonical Function of the Cytoplasmic Poly(A)-Binding Protein

Monika Singh,^{1*}  Bing Ye,² and  Jung Hwan Kim^{1*}

¹Department of Biology, University of Nevada, Reno, Nevada 89557, and ²Life Sciences Institute and Department of Cell and Developmental Biology, University of Michigan, Ann Arbor, Michigan 48109

Dual leucine zipper kinase (DLK) plays a pivotal role in the development, degeneration, and regeneration of neurons. DLK can regulate gene expression post-transcriptionally, but the underlying mechanism remains poorly understood. The *Drosophila* DLK, Wallenda (Wnd), regulates the expression of Down syndrome cell adhesion molecule (Dscam) to control presynaptic arbor growth. This regulation is mediated by the 3' untranslated region (3'UTR) of *Dscam* mRNA, which suggests that RNA binding proteins (RBPs) mediate DLK function. We performed a genome-wide cell-based RNAi screen of RBPs and identified the cytoplasmic poly(A)-binding protein, pAbp, as an RBP that mediates Wnd-induced increase in *Dscam* expression. Genetic analysis shows that Wnd requires *pAbp* for promoting presynaptic arbor growth and for enhancing *Dscam* expression. Our analysis revealed that *Dscam* mRNAs harbor short poly(A) tails. We identified a region in *Dscam* 3'UTR that specifically interacts with pAbp. Removing this region significantly reduced Wnd-induced increase in *Dscam* expression. These suggest that a noncanonical interaction of PABP with the 3'UTR of target transcripts is essential for DLK functions.

Key words: axon growth; DLK; Dscam; PABP; post-transcriptional regulation; RNAi screen

Significance Statement

The kinase DLK plays key roles in a multitude of neuronal responses, including axon development, neurodegeneration, and nerve injury. Previous studies show that DLK acts via mRNAs to regulate protein synthesis, but how DLK does so is poorly understood. This study demonstrates that DLK regulates the synthesis of *Dscam* through the poly(A)-binding protein PABP-C. Whereas PABP-C is known as a general translational activator, our study shows that DLK-mediated *Dscam* expression involves a noncanonical interaction between PABP-C and the *Dscam* mRNA, which leads to a selective regulation of *Dscam* translation by PABP-C. Thus, our study provides novel insights into the mechanisms that underlie the function of DLK and regulation of gene expression of PABP-C.

Received Mar. 15, 2021; revised June 17, 2022; accepted June 22, 2022.

Author contributions: M.S., B.Y., and J.H.K. designed research; M.S. and J.H.K. performed research; J.H.K. contributed unpublished reagents/analytic tools; M.S., B.Y., and J.H.K. analyzed data; and M.S., B.Y., and J.H.K. wrote the paper.

This study was supported by National Institute of Neurological Disorders and Stroke Grant R01NS116463 and National Institute of General Medical Sciences Grant P20GM103440 (Nevada IDeA Network of Biomedical Research Excellence) to J.H.K., National Institute of Mental Health Grant R01MH112669 and National Institute of Neurological Disorders and Stroke Grant R01NS104299 to B.Y., and a grant from the Protein Folding Disease Initiative of the University of Michigan to B.Y. We thank Drs. Catherine Collins, Aaron Goldstrohm, and Silke Dörner for sharing antibodies and DNA constructs; Drs. John Kim and Mallory Freeberg for the initial bioinformatic identification of RNA binding proteins (RBP) in *Drosophila* genome; Dr. Stephanie Mohr and the *Drosophila* RNAi Screening Center for constructing the RBP dsRNA library; the Center for Chemical Genomics at the University of Michigan—Ann Arbor for technical and financial support for the RNAi screen; and the Cellular and Molecular Imaging Core facility at the University of Nevada, Reno, which was supported by National Institutes of Health Grant P20GM103650 and used for research reported in this study.

*M.S. and J.H.K. contributed equally to this work.

Authors declare no competing financial interests.

Correspondence should be addressed to Bing Ye at bingye@umich.edu or Jung Hwan Kim at jungkim@unr.edu.

<https://doi.org/10.1523/JNEUROSCI.0543-21.2022>

Copyright © 2022 the authors

Introduction

The evolutionarily conserved dual leucine zipper kinase (DLK) is a neuronal protein kinase that plays central roles in axon development, synapse maintenance, axon regeneration and degeneration, and neuronal cell death (Nakata et al., 2005; Collins et al., 2006; Xiong et al., 2010; Ghosh et al., 2011; Shin et al., 2012; Klinedinst et al., 2013; Blondeau et al., 2016; Larhammar et al., 2017; Le Pichon et al., 2017). DLK is an upstream mitogen-activated protein kinase (MAP kinase), MAP3K, that activates MAP kinases, including p38 and JNK (Nakata et al., 2005; Collins et al., 2006). The expression changes in genes downstream of these MAP kinases are believed to be central to DLK functions (Collins et al., 2006; Wlaschin et al., 2018; Shin et al., 2019). Interestingly, DLK functions seem to rely on post-transcriptional regulations in different settings. In *Caenorhabditis elegans*, DLK promotes axonal regeneration through stabilizing *CEBP* mRNA in injured axons (Yan et al., 2009). DLK-JNK signal activates an integrated stress response kinase, PERK in mouse, which results in translational

activation of ATF4 for DLK-mediated neuronal cell death (Larhammar et al., 2017). In *Drosophila*, the DLK ortholog Wallenda (Wnd) promotes presynaptic arbor growth by upregulating Down syndrome cell adhesion molecule (Dscam) protein levels (Kim et al., 2013).

Dscam plays critical roles in neuronal development, including the self-avoidance of dendrites in *Drosophila* and mammalian retinal neurons (Fuerst et al., 2008, 2009; Schmucker and Chen, 2009; Zipursky and Sanes, 2010; Schramm et al., 2012) and axon guidance and growth (Kim et al., 2013; Alavi et al., 2016; Bruce et al., 2017; Santos et al., 2018). Dscam has also been implicated in various brain disorders (Amano et al., 2008; Shen et al., 2011; O’Roak et al., 2014). Thus, the regulation of Dscam expression is important for understanding neuronal development and brain disorders. Our previous study discovered that Wnd does not change the abundance of Dscam mRNA but requires the 3′ untranslated region (3′ UTR) of Dscam for this regulation (Kim et al., 2013). This suggests that Wnd enhances the mRNA translation of Dscam. As a protein kinase, DLK likely requires an RNA-binding protein (RBP) to control protein translation through 3′ UTR. However, the identity of the RBP is unknown.

Through an unbiased RNAi screen, we have identified pAbp, *Drosophila* ortholog of the cytoplasmic Poly(A)-binding protein (PABP-C) as an RBP that is required for Wnd-induced upregulation of Dscam expression as well as for Wnd-induced axon arborization. Although PABP-C is considered as a general activator of protein translation through poly(A) tail interaction (Munroe and Jacobson, 1990); it also performs gene-specific post-transcriptional regulations (Wu and Bag, 1998; Lyabin et al., 2011; Vazquez-Pianzola et al., 2011; Eliseeva et al., 2012; Iwakawa et al., 2012; Smith et al., 2017). We identified an adenine nucleotide rich (A-rich) region in the 3′ UTR of Dscam that mediates pAbp interaction. Deletion of this region significantly reduced Wnd-induced Dscam expression both *in vitro* and *in vivo*. We further show that Dscam mRNA has significantly short poly(A) tails. Our study demonstrates that DLK function relies on the noncanonical mRNA interaction of PABP-C. It identifies not only a novel mechanism that mediates DLK signaling but also one that underlies the post-transcriptional regulation of Dscam expression.

Materials and Methods

Drosophila melanogaster strains. *Drosophila* strains were kept under standard condition at 25°C in a humidified chamber. The following strains were used in this study: *w¹¹¹⁸* (stock #3605, Bloomington Drosophila Stock Center), *ppk-GAL4* (Grueber et al., 2007), *UAS-Dscam[TM2]::GFP-Dscam-3′ UTR* (ectodomain 3.36.25) and *UAS-Dscam[TM2]::GFP* (ectodomain 3.36.25; Kim et al., 2013), *hiw^{AN}* (Wu et al., 2005), *pAbp^{EP310}* (stock #17261, Bloomington Drosophila Stock Center) and *pAbp^{K10109}* (stock #10970, Bloomington Drosophila Stock Center; Sigrist et al., 2000), *UAS-FRT-rCD2-STOP-FRT-mCD8::GFP* (Yang et al., 2014), and *UAS-pAbp* (stock #914, Bloomington Drosophila Stock Center).

FRT^{G13}, *UAS-mCD8::GFP*, *pAbp^{K10109}* was generated through recombination. The primers used for genotyping *pAbp^{K10109}* were *pAbp^{K10109}-top* (GAGGGCGCAACGCACGACAA) and *pAbp^{K10109}-bottom* (ATATAA TCATGTGTGTGTGTACACACTGGC).

Axon arborization analysis. The mosaic analysis with a repressible cell marker (MARCM) technique for presynaptic arbor analysis (Kim et al., 2013) and the quantitation of axon arborization by counting the axonal connecting fibers (Sterne et al., 2015) were done as previously described.

DNA constructs and Drosophila transgenic flies and Schneider 2 cell transfection. The enhanced green fluorescent protein (EGFP) reporters for RNAi screen were reported previously (Kim et al., 2013). To generate

Wnd-HSL (histone-stem-loop), the Wnd-*Wnd-3′ UTR* sequence without polyadenylation signal (PAS) was recovered from UAS-Wnd (Collins et al., 2006) via PCR and inserted proximal to HSL sequence into pAC5.1-Rn-Luc-HSL (Weidmann et al., 2014) using the NdeI and StuI restriction sites. Wnd-*Wnd-3′ UTR*-HSL sequence was then transferred into pUAST-HA using EagI and XhoI sites, followed by transferring HA-Wnd-*Wnd-3′ UTR*-HSL into the pAttB vector (Bischof et al., 2007) using NotI and XbaI sites. UAS-*Dscam-5′ UTR*-Dscam-Dendra2-SV40-3′ UTR was generated in pUASTattB (Bischof et al., 2007). UAS-*Dscam-5′ UTR*-Dscam-Dendra2-*Dscam-3′ UTR* and UAS-*Dscam-5′ UTR*-Dscam-Dendra2-*Dscam-3′ UTR*ΔpAbp were generated in pAttB (Bischof et al., 2007). The 5′ UTR and 3′ UTR of *Dscam* were obtained from *w¹¹¹⁸* genomic DNA by PCR. The Dscam coding sequence was from UAS-Dscam[TM2]::GFP (ectodomain 3.36.25). *Dscam-3′ UTR*ΔpAbp was generated by a site-directed mutagenesis. The resulting PCR products were ligated together using an In-Fusion Cloning Kit (Clontech) following instructions of the manufacturer. UAS-*DSCAM-SV40-3′ UTR* with the A-rich region from *Dscam-3′ UTR* was generated in pUASTattB (Bischof et al., 2007). The 123-bp A-rich sequence was recovered from UAS-*Dscam-UTR*-Dscam-Dendra2-*Dscam-3′ UTR* via PCR and inserted at 148 bp upstream of the polyadenylation signal in SV40-3′ UTR using an In-Fusion Cloning Kit (Clontech) following directions of the manufacturer. Transgenic flies were generated by PhiC31-mediated germline transformation (Bischof et al., 2007).

Schneider 2 cell culture, transfection, and Western blot analysis. Schneider 2 (S2) cells were maintained in *Drosophila* Schneider’s Medium (Thermo Fisher Scientific) supplemented with 10% fetal bovine serum (Sigma-Aldrich) at 27°C in a humidified incubator. Cells were transfected with indicated DNA constructs along with tubulin-Gal4 (Lee and Luo, 2001) using Lipofectamine 2000 (Life Technologies) following instructions from the manufacturer. For Western blot analysis, S2 cells were washed two times with PBS. The whole lysates were resolved on 8% SDS-PAGE gels and subjected to Western blot analysis as previously described (Kim et al., 2013). Primary antibodies used were rabbit polyclonal anti-Wnd (Collins et al., 2006), rabbit polyclonal anti-pAbp (Antic et al., 2015), rabbit polyclonal anti-Dendra2 (Antibodies-online), mouse monoclonal anti-tubulin (DM1A, Sigma-Aldrich), mouse monoclonal anti-puromycin (12D10, Sigma-Aldrich), Rat Anti-Elav (catalog #7E8A10, Developmental Studies Hybridoma Bank).

The validation of Rabbit polyclonal anti-pAbp antibody was done using S2 cells that were treated with pAbp dsRNA (7.5 μg) in a 24 well plate for 4 d. Cells were harvested. Total cell lysates were resolved in SDS-PABP before Western analysis (Fig. 6D).

RNAi screening. The RBP-RNAi library (Mohr et al., 2015) was obtained from the *Drosophila* RNAi Screening Center (DRSC). The screening was done in a duplicate, nonadherent 384-well plate format. S2 cells were plated directly in the wells that contain individual dsRNAs (0.25 μg) and cultured for 24 h before transfecting with UAS-Wnd along with EGFP-*Dscam-3′ UTR* reporter. Plates were inverted and kept at 27°C in a humidified incubator to prevent excessive culture media evaporation. After 48 h post-transfection, the average intensity of green fluorescence from individual cells was measured using a high-throughput flow cytometry, the HyperCyt System (Intellicyt). A *lacZ* dsRNA was used as a negative control. The *lacZ* dsRNAs were placed in seven wells that were scattered through each 384-well plate. The average GFP intensity values from the seven *lacZ* dsRNA-treated wells were used to generate an average GFP intensity (AVE-GFP_{lacZ}) and an SD (SD_{lacZ}). The initial hits were selected if GFP_{RBP} < AVE-GFP_{lacZ} - 1.5 × SD_{lacZ}, where GFP_{RBP} refers to the average GFP intensity from the cells that were treated with individual RBP dsRNA. The hits were finalized only when the duplicate wells for a given RBP dsRNA were both selected by the criteria.

For the secondary screening, the dsRNAs from the initial hits were synthesized from the DRSC DNA templates using TranscriptionAid T7 High Yield Transcription Kit (Thermo Fisher Scientific) and purified using Quick-RNA Miniprep Kit (Zymo Research). S2 cells were bath incubated with individual dsRNAs for 24 h before transfecting with UAS-Wnd along with EGFP-SV40-3′ UTR or EGFP-*Dscam-3′ UTR*. The GFP intensity was measured 48 h after transfection.

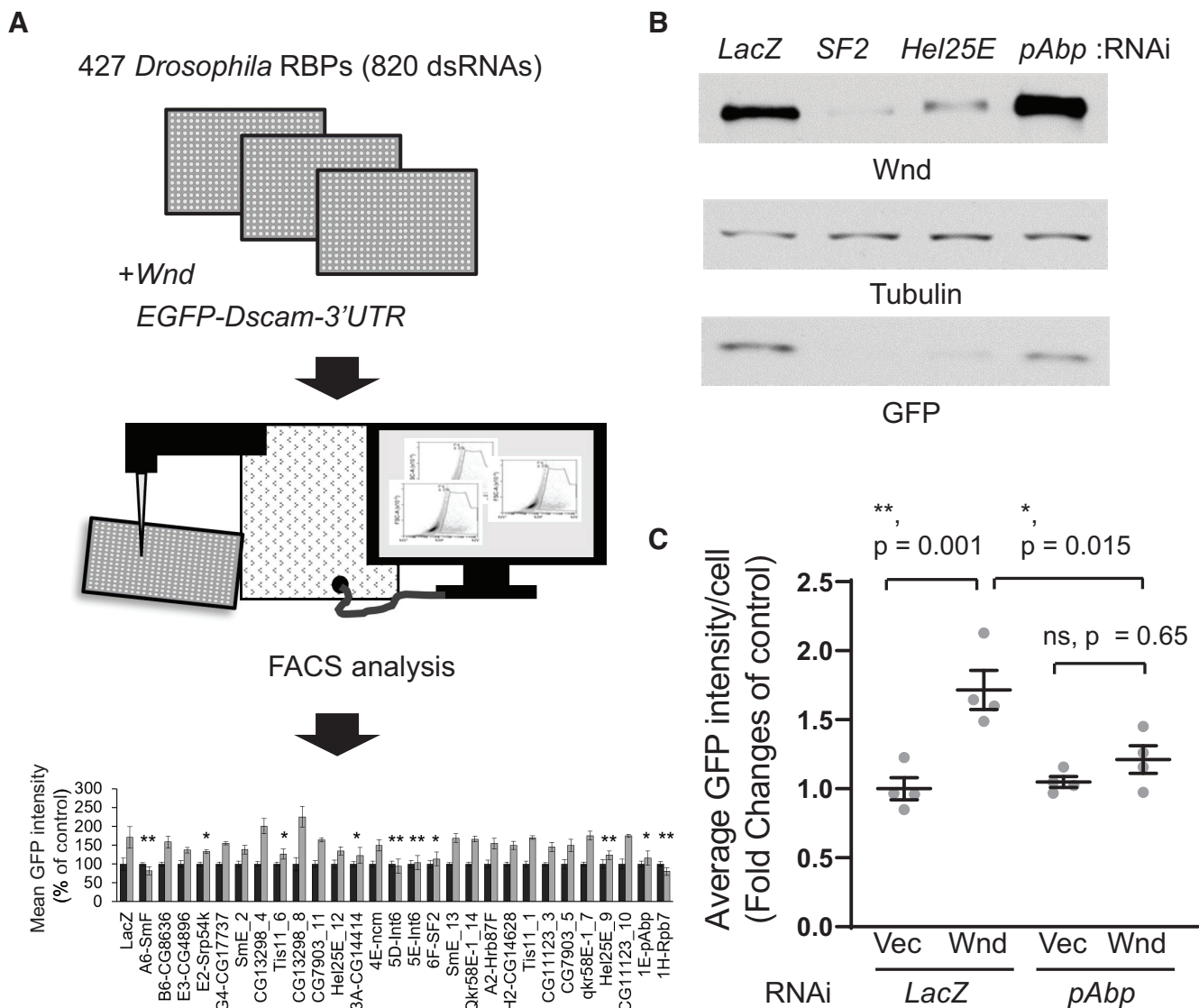


Figure 1. Genome-wide cell-based RNAi screen identifies pAbp as an RBP that mediates Wnd-induced increase in Dscam expression. **A**, Cell-based RNAi screen. S2 cells were treated with the dsRNA library against *Drosophila* RBP genes and transfected with Wnd and EGFP-*Dscam*-3'UTR reporter constructs, followed by high-throughput flow cytometry analysis. Bottom, The results of the secondary screen. dsRNA-treated cells were transfected with EGFP-*Dscam*-3'UTR reporter constructs along with an empty vector (back bar) or with Wnd construct (gray bar). The empty vector control was used to normalize values for each dsRNA ($n = 4$). LacZ dsRNA was used as a control. The data shown are an example from the screening. Mean \pm SEM; * $p < 0.05$, ** $p < 0.01$, two-tailed, unpaired t test. **B**, *pAbp* RNAi does not reduce Wnd expression in S2 cells. Cell lysates obtained from the secondary screen was tested by Western blot analysis. Note that Wnd expression was largely decreased in SF2 and Hel25E RNAi-treated cells. *pAbp* RNAi did not affect Wnd expression, although it did reduce GFP expression from EGFP-*Dscam*-3'UTR reporter. Tubulin blot was used as a loading control. **C**, *pAbp* RNAi blunts Wnd-induced increase in EGFP-*Dscam*-3'UTR reporter. S2 cells were treated with *pAbp* dsRNA or with LacZ dsRNA before transfecting with EGFP-*Dscam*-3'UTR construct along with an empty vector (Vec) or Wnd construct ($n = 4$). The average GFP intensity was measured using flow cytometry. The data were expressed as mean \pm SEM. One-way ANOVA ($F_{(3,12)} = 11.25$, $p = 0.0008$) followed by *post hoc* Tukey's multiple comparison test. The p values from Tukey's test are indicated in the graph * $p < 0.05$, ** $p < 0.01$, ns = not significant.

RNP pulldown. The biotinylated, single-stranded *Dscam*-3'UTR, SV40-3'UTR, and *Dscam*-3'UTR Δ pAbp RNA were generated using TranscriptionAid T7 High Yield Transcription Kit (Thermo Fisher Scientific) with Biotin-16-UTP (Sigma-Aldrich). The T7 sequence was used for *in vitro* transcription reaction. RNAs were purified using Quick-RNA Miniprep Kit (Zymo Research). All RNAs contain S1 aptamer sequence (Srisawat and Engelke, 2001) at their 5'-end for better Streptavidin bead coupling. RNAs were incubated with Streptavidin agarose (Thermo Fisher Scientific) in binding buffer (50 mM HEPES, pH7.4, 300 mM NaCl, 0.5% NP-40, 2 mM MgCl₂, 1 mM DTT) in the presence of RNaseOUT (Invitrogen) for 1 h at 4°C. Unbound RNA was removed by washing the beads three times with binding buffer. An aliquot of RNA-bound Streptavidin agarose was transferred to a new tube that contained 100 ng firefly luciferase RNA. The agarose bead-bound RNA was extracted using Trizol (Thermo Fisher Scientific), resolved, and quantified on 1.5% formaldehyde-denaturing agarose gel using firefly luciferase RNA as an extraction and a loading control.

S2 cells were washed two times with PBS before being lysed for 30 min in ice-cold binding buffer containing EDTA-free protease inhibitor cocktail (Research Products International). The crude lysates were centrifuged at 1000 \times g, 4°C, for 5 min. The resulting postnuclear supernatant was supplemented with SUPERase-In (Thermo Fisher Scientific) and further centrifuged at 22,000 \times g, 4°C, for 20 min. The resulting lysates were precleared with Streptavidin agarose for 1 h at 4°C, incubated with the RNA-coupled Streptavidin agarose for 2 h at 4°C. The RNP complexes were washed five times with binding buffer before resolved on 8% SDS-PAGE gel and subsequent Western blot analysis.

Immunostaining. *Drosophila* third instar larvae were prepared as previously described (Kim et al., 2013). Primary antibodies used were chicken polyclonal anti-GFP (Aves Labs), rabbit polyclonal anti-Dendra2 (Antibodies-online), and rabbit polyclonal anti-RFP (Rockland Immunochemicals). The secondary antibodies used were Cy2- or Cy5-conjugated goat anti-chicken and Cy2- or Cy5-conjugated

goat anti-rabbit (Jackson ImmunoResearch). The imaging was done with a Leica SP5 confocal system or a custom-built spinning disk confocal microscope equipped with a 63× oil-immersion objective with a 0.3 μm step size. The resulting 3D images were projected into 2D images using a maximum projection method in ImageJ software. A region of interest was drawn in the cell body of C4da neurons, and the mean fluorescence intensity was measured using ImageJ software to quantify *UAS-Dscam* transgene expression levels. Because the activity of GAL4 varies among individual neurons, the mean fluorescence intensity of *UAS-mCD8::GFP* or *UAS-mCD8::mRFP* transgene expression was measured from the same region of interest and used as a normalization control.

Puromycylation assay. The batches of 20 brains were harvested from third instar larvae in ice-cold PBS. PBS was removed after centrifugation at 4°C, and 1 ml HL3 (hemolymph-like) solution was added containing the following (in mM): 5 HEPES, pH 7.2, 70 NaCl, 5 KCl, 0.5 CaCl₂, 20 MgCl₂, 5 trehalose, and 115 sucrose containing 10 μg/ml puromycin (Thermo Fisher Scientific). Larval samples were then incubated in a nutator for 15 min at room temperature (RT). Following incubation, HL3 solution was removed after a brief centrifugation at RT. Larval brains were washed three times with ice-cold PBS before resolved on 10% SDS-PAGE gel and subsequent Western blot analysis.

Poly(A) tail measurement. The G/I (guanosine/inosine) tailing takes advantage of a yeast poly(A) polymerase that incorporates additional nucleotides at the very 3'-end of RNAs, and thus preserves the 3'-end of RNA. After the addition of repeating G and I nucleotides, cDNA is prepared using a universal reverse primer. PCR is performed with the PCR primers that anneal to the 3'UTR from the genes of interest to detect the gene-specific as well as the gene-specific poly(A) products. The PCR products were analyzed by Agilent 2100 Bioanalyzer high-resolution capillary gel electrophoresis. Total RNA was extracted using Quick-RNA Microprep Kit (Zymo Research). The quality and quantity of isolated RNA was monitored by denaturing 1.5% agarose gel electrophoresis and spectrophotometry. Guanosine and inosine residues were added in the 3'-end of the poly(A)-containing RNAs followed by cDNA synthesis using the newly added G/I tails as priming sequence using the Poly(A) Tail-Length Assay Kit (Thermo Fisher Scientific) following instructions of the manufacturer. A gene-specific forward/reverse primer set right upstream of the polyadenylation site was used to generate a PCR product. A primer set with a gene-specific forward and the universal reverse primer was used to generate a product that includes the poly(A) tails of the gene of interest. The poly(A) tail lengths of the gene of interest are the sizes of poly(A) PCR products minus the calculated length of the gene-specific forward primer to the putative polyadenylation site. The sizes of the PCR products were analyzed by Agilent 2100 Bioanalyzer high resolution capillary gel electrophoresis with Agilent 2100 software.

The primers used are the following: *Dscam*-forward (CGCAGCCAC AACAATTGAATG), *Dscam*-reverse (AAAATAAAATCAAATCATAT

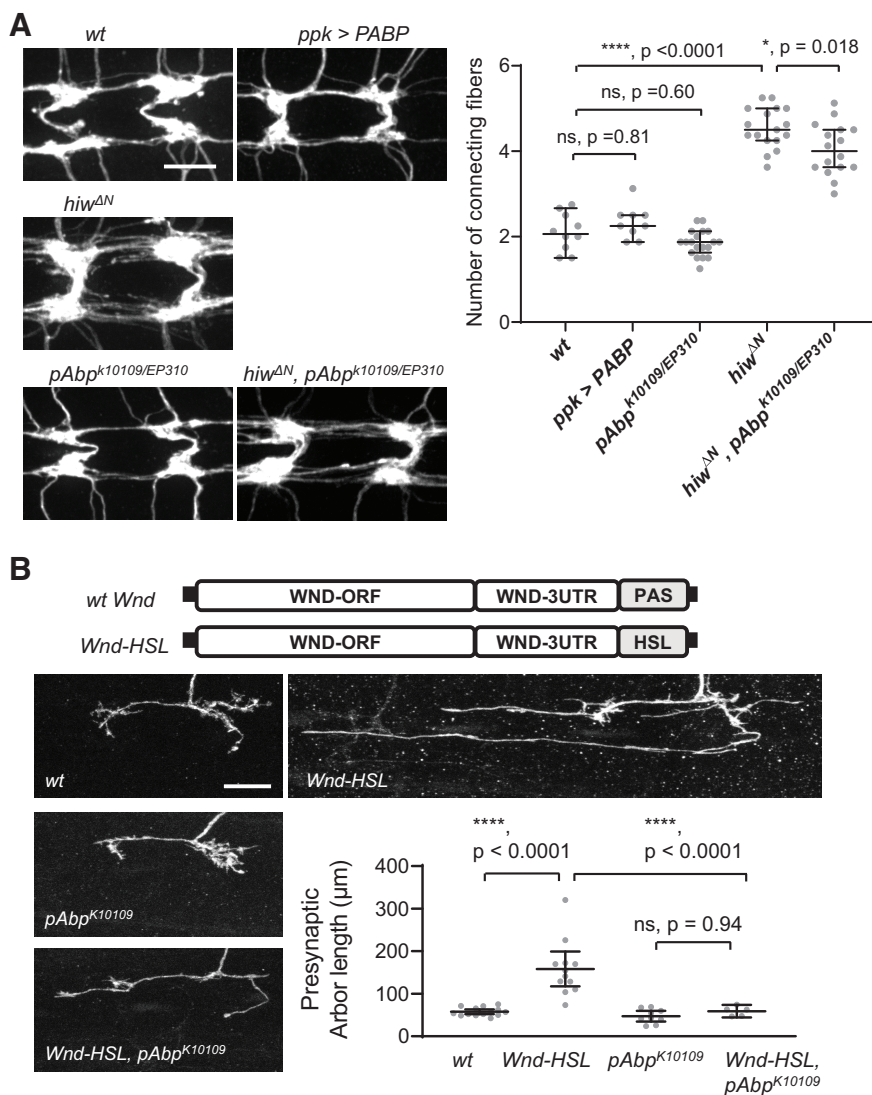


Figure 2. *pAbp* is required for Wnd-induced exuberant presynaptic arborization. **A**, The axon terminals from C4da neurons that correspond to abdominal segments 4 and 5 were visualized with *mCD8::RFP* using *ppk-Gal4* (left). Hemizygous male *hiw* mutant (*hiw*^{ΔN}) and male wild-type (*w*¹¹¹⁸; *ppk-GAL4*, *UAS-mCD8::RFP/+*) animals were used. The average number of neuropil-connecting fibers was counted from each animal (abdominal segments 4–6) and expressed as median ± 95% CI (right). One-way ANOVA ($F_{(4,66)} = 114.6$, $p < 0.0001$) followed by *post hoc* Tukey's multiple comparison test. The *p* values from Tukey's test are indicated in the graph. Sample numbers were *wt* (*w*¹¹¹⁸; *ppk-GAL4*, *UAS-mCD8::RFP/+*) ($n = 10$), *ppk > PABP* (*w*¹¹¹⁸; *ppk-GAL4*, *UAS-mCD8::RFP/PABP*) ($n = 9$), *pAbp*^{K10109/EP310 (*w*¹¹¹⁸; *pAbp*^{K10109}/*pAbp*^{EP310}, *ppk-GAL4*, *UAS-mCD8::RFP/+*) ($n = 19$), *hiw*^{ΔN} (*hiw*^{ΔN}; *ppk-GAL4*, *UAS-mCD8::RFP/+*) ($n = 17$), *hiw*^{ΔN}, *pAbp*^{K10109/EP310} (*hiw*^{ΔN}; *pAbp*^{K10109}/*pAbp*^{EP310}; *ppk-GAL4*, *UAS-mCD8::RFP/+*) ($n = 16$). *wt*, Wild type. Scale bar, 10 μm. **B**, Schematic of Wnd-HSL. Wnd-HSL contains HSL instead of PAS in its 3'UTR, which makes Wnd protein expression independent of poly(A) tail. The MARCM analysis was performed to visualize the presynaptic arbors from individual C4da neurons. Transgenes were expressed using a C4da-specific *ppk-GAL4*. Presynaptic arbors were visualized with a membrane marker *mCD8::GFP* transgene. Overexpressing Wnd-HSL caused a dramatic increase in presynaptic arbor length in *wt* C4da neurons, but not in *pAbp*^{K10109} C4da neurons. The *pAbp* mutation alone did not significantly affect presynaptic arborization. Sample numbers were *wt* (*hs-FLP*, *y*, *w*¹¹¹⁸/*w*¹¹¹⁸, *FRT*^{G13}, *UAS-mCD8::GFP/FRT*^{G13}, *GAL80*; *ppk-GAL4*, *UAS-mCD8::GFP/+*) ($n = 14$), *Wnd-HSL* (*hs-FLP*, *y*, *w*¹¹¹⁸/*w*¹¹¹⁸, *FRT*^{G13}, *UAS-mCD8::GFP/FRT*^{G13}, *GAL80*; *ppk-GAL4*, *UAS-mCD8::GFP/UAS-Wnd-HSL*) ($n = 12$), *pAbp*^{K10109} (*hs-FLP*, *y*, *w*¹¹¹⁸/*w*¹¹¹⁸, *FRT*^{G13}, *UAS-mCD8::GFP*, *pAbp*^{K10109}/*FRT*^{G13}, *GAL80*; *ppk-GAL4*, *UAS-mCD8::GFP/+*) ($n = 12$), *Wnd-HSL* in *pAbp*^{K10109} (*hs-FLP*, *y*, *w*¹¹¹⁸/*w*¹¹¹⁸, *FRT*^{G13}, *UAS-mCD8::GFP*, *pAbp*^{K10109}/*FRT*^{G13}, *GAL80*; *ppk-GAL4*, *UAS-mCD8::GFP/UAS-Wnd-HSL*) ($n = 5$). The data were expressed as median ± 95% CI. One-way ANOVA ($F_{(3,36)} = 21.91$, $p < 0.0001$) followed by *post hoc* Tukey's multiple comparison test. The *p* values from Tukey's test are indicated in the graph * $p < 0.05$, **** $p < 0.0001$, ns = not significant. Scale bar, 10 μm.}

ATTAGCAACTTATGAAC), GAPDH2-forward (CACTTCAGAAAC GGCCTGAAAATGGC), GAPDH2-reverse (AAATATTTAAATGCT TATGAGTCGGCATTTTTAAAACTAC), and the universal-reverse (GGTAATACGACTCACTATAGCGAGACCCCCCCCCCTT).

Experimental design and statistical analysis. All statistical analysis was performed as two-tailed using GraphPad Prism software version

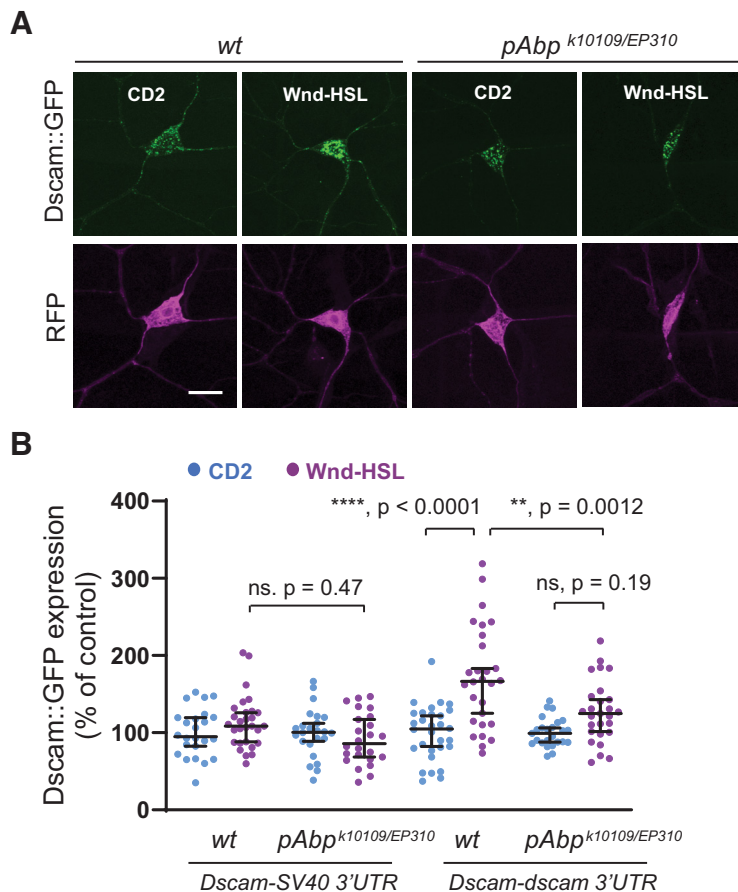


Figure 3. *pAbp* is required for Wnd-induced *Dscam* expression. **A**, Wnd-HSL or a control transgene, CD2, was expressed in the larval C4da neurons along with *Dscam::GFP-SV40-3'UTR* or *Dscam::GFP-Dscam-3'UTR* in wild-type (*wt*) control (w^{1118}) or in *pAbp* mutants ($pAbp^{k10109/EP310}$). The cell bodies of C4da neurons are shown, *Dscam::GFP* (green) and *mCD8::RFP* (magenta). Scale bar, 10 μ m. Expression of *Dscam* in *Dscam::GFP-SV40-3'UTR* not shown. **B**, The expression levels of *Dscam::GFP* were measured from the individual C4da cell bodies. An *mCD8::RFP* (RFP) transgene was used to normalize *Dscam::GFP* intensity. The data were expressed as median \pm 95% CI. Note that the increase in *Dscam::GFP* expression from *Dscam::GFP-Dscam-3'UTR* is significantly higher in *Wnd-HSL* than in *Wnd-HSL*, $pAbp^{k10109/EP310}$; one-way ANOVA ($F_{(7,203)} = 12.03$, $p < 0.0001$) followed by *post hoc* Tukey's multiple comparison test. Sample numbers were *Dscam::GFP-SV40-3'UTR* and CD2 (w^{1118} , $GAL4^{4-77}/UAS-Dscam::GFP-SV40-3'UTR$; $UAS-FRT-rCD2-STOP-FRT-mCD8::GFP/+$) ($n = 24$), *Dscam::GFP-SV40-3'UTR* and *Wnd-HSL* (w^{1118} , $GAL4^{4-77}/UAS-Dscam::GFP-SV40-3'UTR$; $UAS-Wnd-HSL/+$) ($n = 29$), *Dscam::GFP-SV40-3'UTR* and CD2 in $pAbp^{k10109/EP310}$ (w^{1118} , $GAL4^{4-77}$, $pAbp^{k10109}/pAbp^{EP310}$, $UAS-Dscam::GFP-SV40-3'UTR$; $UAS-FRT-rCD2-STOP-FRT-mCD8::GFP/+$) ($n = 29$), *Dscam::GFP-SV40-3'UTR* and *Wnd-HSL* in $pAbp^{k10109/EP310}$ (w^{1118} , $GAL4^{4-77}$, $pAbp^{k10109}/pAbp^{EP310}$, $UAS-Dscam::GFP-SV40-3'UTR$; $UAS-Wnd-HSL/+$) ($n = 32$), *Dscam::GFP-Dscam-3'UTR* and CD2 (w^{1118} , $GAL4^{4-77}/UAS-Dscam::GFP-Dscam-3'UTR$; $UAS-FRT-rCD2-STOP-FRT-mCD8::GFP/+$) ($n = 30$), *Dscam::GFP-Dscam-3'UTR* and *Wnd-HSL* (w^{1118} , $GAL4^{4-77}/UAS-Dscam::GFP-Dscam-3'UTR$; $UAS-Wnd-HSL/+$) ($n = 28$), *Dscam::GFP-Dscam-3'UTR* and CD2 in $pAbp^{k10109/EP310}$ (w^{1118} , $GAL4^{4-77}$, $pAbp^{k10109}/pAbp^{EP310}$, $UAS-Dscam::GFP-Dscam-3'UTR$; $UAS-FRT-rCD2-STOP-FRT-mCD8::GFP/+$) ($n = 33$), *Dscam::GFP-Dscam-3'UTR* and *Wnd-HSL* in $pAbp^{k10109/EP310}$ (w^{1118} , $GAL4^{4-77}$, $pAbp^{k10109}/pAbp^{EP310}$, $UAS-Dscam::GFP-Dscam-3'UTR$; $UAS-Wnd-HSL/+$) ($n = 30$). The *p* values from Tukey's test are indicated in the graph ** $p < 0.01$, **** $p < 0.0001$, ns = not significant.

7.04. The Mann–Whitney test was used for presynaptic arbor analysis (see Fig. 2) and immunostaining results (see Figs. 3, 9). An unpaired Student's *t*-test was used for S2 cell RNAi (Fig. 1), poly(A) length measurement (see Fig. 5), and Western blot analysis (see Figs. 4, 6, 7, 8). For multigroup comparisons, one-way ANOVA was used followed by *post hoc* Tukey's multiple comparisons test. A *p* value smaller than 0.05 was considered statistically significant. All *p* values are indicated as not significant; * $p < 0.05$, ** $p < 0.01$, *** $p < 0.001$, and **** $p < 0.0001$.

Results

Genome-wide cell-based RNAi screen identifies *pAbp* as an RBP that mediates Wnd-induced increase in *Dscam* expression
Our previous work has shown that Wnd post-transcriptionally regulates the expression of *Dscam* through the 3'UTR of *Dscam*

without affecting the abundance of *Dscam* mRNA, which suggests the role of Wnd in *Dscam* translation (Kim et al., 2013). The study also suggested that the increased *Dscam* expression mediates the effect of Wnd on increased presynaptic axon arbors (Kim et al., 2013). However, how Wnd controls *Dscam* translation was unclear. Wnd may require an RBP for this regulation as Wnd, as a protein kinase, unlikely affects the 3'UTR of mRNAs directly. In search for such RBPs, an unbiased cell-based RNAi screen was performed in cultured *Drosophila* S2 cells. We took advantage of an EGFP reporter that recapitulated Wnd-mediated *Dscam* expression regulation in S2 cells (Kim et al., 2013). We used a dsRNA library for all annotated *Drosophila* RBPs (Mohr et al., 2015). In total, 820 individual dsRNAs against 427 *Drosophila* RBP genes were screened. S2 cells were plated in a microplate and bath incubated with individual dsRNAs to knock down RBP genes before transfecting an EGFP-*Dscam* 3'UTR construct either with a Wnd expression construct or an empty DNA construct. A dsRNA against *lacZ* was used as a negative control. The expression levels of EGFP were assessed 48 h post-transfection by a high-throughput flow cytometry analysis (Fig. 1A). The initial screen generated multiple hits in 18 RBP genes. We then performed a secondary screening using a control EGFP reporter that contains the 3'UTR from *SV40* (Fig. 1A, bottom) and narrowed down to nine candidates. An RBP RNAi may decrease reporter expression by inhibiting plasmid gene expression or by reducing Wnd expression. To rule out these possibilities, we performed an additional test using Western blotting with an anti-Wnd antibody and obtained four RBPs as the final candidates, namely, *pAbp*, *Int6*, *Rpb7*, and *CG14414*. *CG14414* has neither a known function nor is orthologous to any known mammalian genes. Three final hits have known roles in translation initiation. *Int6* encodes the eukaryotic translation initiation factor 3 subunit E, eIF3e, which is involved in translation initiation (Akiyoshi et al., 2001). *Rpb7* encodes a nonessential component of RNA-polymerase

II that is involved in diverse functions including translation initiation (Harel-Sharvit et al., 2010). *pAbp* is a *Drosophila* ortholog of PABP-C. We selected *pAbp* for further study because of its well-characterized role in translation initiation (Munroe and Jacobson, 1990). Moreover, *pAbp* RNAi did not reduce Wnd expression (Fig. 1B) but significantly reduced Wnd-triggered increase in EGFP expression from the EGFP-*Dscam*-3'UTR reporter (Fig. 1C).

pAbp* is required for Wnd-induced *Dscam* translation *in vivo
Wnd increases the size of presynaptic axon arbors by enhancing *Dscam* expression in *Drosophila* larval class IV dendritic arborization (C4da) neurons (Kim et al., 2013). To evaluate the

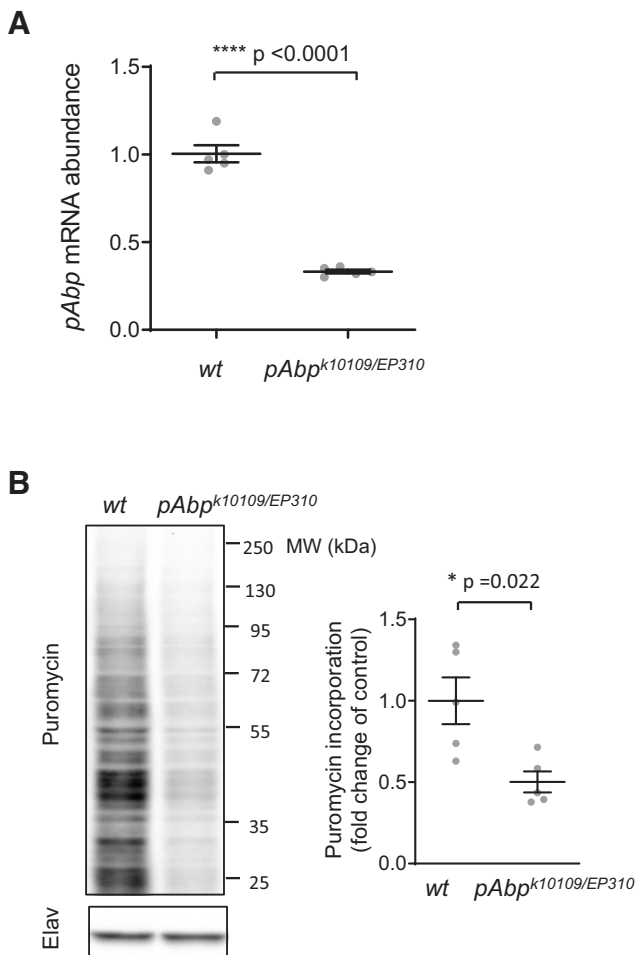


Figure 4. Characterization of *pAbp*^{K10109/EP310}. **A**, Total RNAs extracted from the wandering third instar larval brains from a wild-type (*wt*) control (*w*¹¹⁸) and *pAbp*^{K10109/EP310} were subjected to RT-qPCR to measure *pAbp* mRNA abundance. The *pAbp* mRNA levels were normalized to *GAPDH1* mRNA levels via the 2^{ΔΔCT} method. The heterozygote combination of *pAbp*^{K10109} and *pAbp*^{EP310} alleles reduced by ~65% *pAbp* mRNA abundance. A similar result was obtained using an independent qPCR primer pair. The data were expressed as mean ± SEM of five technical replicates ($t = 13.47$, $df = 4.383$, $p < 0.0001$, 2-tailed Welch's t test). **B**, Puromycylation to measure protein synthesis rate. The wandering third instar larval brains from a *wt* control (*w*¹¹⁸) and *pAbp*^{K10109/EP310} were briefly incubated in puromycin and subjected to Western blot analysis with anti-puromycin antibody. Anti-Elav blot was used as a loading control. The incorporation of puromycin was displayed as mean ± SEM of five biological replicates ($t = 3.167$, $df = 8$, $p = 0.022$, 2-tailed Welch's t test) * $p < 0.05$, **** $p < 0.0001$.

functional role of pAbp in this process, we first examined the axonal arborization of C4da neurons in pAbp overexpression (Fig. 2A). The C4da neuron axon arborization was measured by counting the number of fibers connecting the segmentally repeated neurophils. The method was successfully used before (Wang et al., 2013; Sterne et al., 2015). We did not observe any changes, which suggests that pAbp is expressed sufficiently under normal condition. We then tested the effect of *highwire* (*hiw*)-induced axon arborization by *pAbp* mutations. *Hiw* normally degrades Wnd expression to suppress axonal arborization (Collins et al., 2006). Thus, increased Wnd expression causes excessive axon arborization in an *hiw* loss-of-function allele (*hiw*^{ΔN}). Because strong loss-of-function alleles of *pAbp* caused larval lethality, we used a transheterozygous combination of two *pAbp* hypomorphic alleles—partial loss of function *pAbp*^{K10109} and *pAbp*^{EP310}—to study the effects of loss of *pAbp*. The mutation of *hiw* caused a dramatic increase in axon

arborization, which was mildly but significantly reduced by *pAbp* mutations (21% rescue; Fig. 2A).

PABP-C binds to the poly(A) tails of mRNAs and interacts with mRNA translation initiation complex (Wells et al., 1998). As virtually all cellular mRNAs contain a poly(A) tail, PABP-C is considered as a general mRNA translation activator. A poly(A) tail addition is triggered by a *cis*-element at mRNA 3'UTR, also known as PAS. Histone mRNA is an exception because it does not contain a PAS. Instead, HSL sequence marks the transcriptional termination and recruits stem loop binding protein (SLBP). Through binding to HSL, SLBP plays a similar role as PABP-C to histone mRNA (Sánchez and Marzluff, 2002; Marzluff et al., 2008). To examine the role of pAbp in Wnd-mediated Dscam regulation *in vivo*, we generated a *Wnd* transgene to dissociate its expression from the pAbp regulation by replacing the PAS of *Wnd* mRNA to HSL sequences (Fig. 2B). In this transgene, *Wnd*-HSL, Wnd expression is through the HSL mechanism and is thus independent of the canonical *pAbp* function via poly(A) tail interaction. We performed the mosaic analysis with a repressible cell marker (MARCM; Lee and Luo, 2001) in wild-type and *pAbp* mutant larval C4da neurons that are expressing *Wnd*-HSL. MARCM allowed us to use a strong loss-of-function allele of *pAbp*, *pAbp*^{K10109}, without causing larval lethality. As shown in Figure 2B, the expression of *Wnd*-HSL induced a dramatic increase in presynaptic arbor size, which was almost completely abolished by *pAbp* mutations. These results strongly suggest that pAbp mediates Wnd-induced axon terminal growth, which is through *Dscam* (Kim et al., 2013).

Having a tool for directly testing a role of pAbp in Wnd-induced Dscam regulation, we then asked whether Wnd controls Dscam expression through pAbp. The *Wnd*-HSL transgene was expressed by using the GAL4-UAS bipartite expression system in the C4da neurons with *GAL4*⁴⁻⁷⁷ in wild-type and in *pAbp* mutant (*pAbp*^{K10109/EP310}) animals. As expected, Wnd-HSL increased expression of a Dscam transgene that contains *Dscam*-3'UTR but not the one with *SV40*-3'UTR (Fig. 3A,B). Importantly, this effect was significantly abolished by the loss of *pAbp*, which suggests that pAbp is required for Wnd-induced *Dscam* translation *in vivo*.

Dscam mRNA contains short poly(A) tails

How does PABP as a general translation activator exhibit selectivity for *Dscam*? And, what is the extent of this selectivity? To answer these questions, we first measured how much pAbp function is lost in the hypomorphic transheterozygote of the *pAbp*^{K10109} and *pAbp*^{EP310} alleles. We performed quantitative real-time PCR on the larval brains from wild type and *pAbp*^{K10109/EP310} and found a dramatic reduction (67%) in *pAbp* mRNA abundance (Fig. 4A). Although this clearly demonstrates a reduction in *pAbp* mRNA levels, pAbp proteins may exist in excess, and their functions be consequently unaffected by in *pAbp*^{K10109/EP310}. Therefore, we decided to measure general protein synthesis, a proxy for pAbp function, using the puromycylation assay. Puromycylation takes advantage of puromycin, an amino-nucleoside antibiotic. Puromycin resembles a charged-tRNA and causes termination of mRNA translation by incorporating itself into a growing polypeptide chain from ribosomes (Pestka, 1971). Specific antibodies against puromycin allow the evaluation of the puromycin incorporation rate, which linearly correlates to the mRNA translation rate (Eggers et al., 1997). The larval brains from wild type and *pAbp*^{K10109/EP310} were isolated and briefly treated with puromycin at a low concentration. Western blot analysis was performed on the brain lysates using anti-puromycin antibody. The result showed a 50% reduction in the general protein synthesis rate in

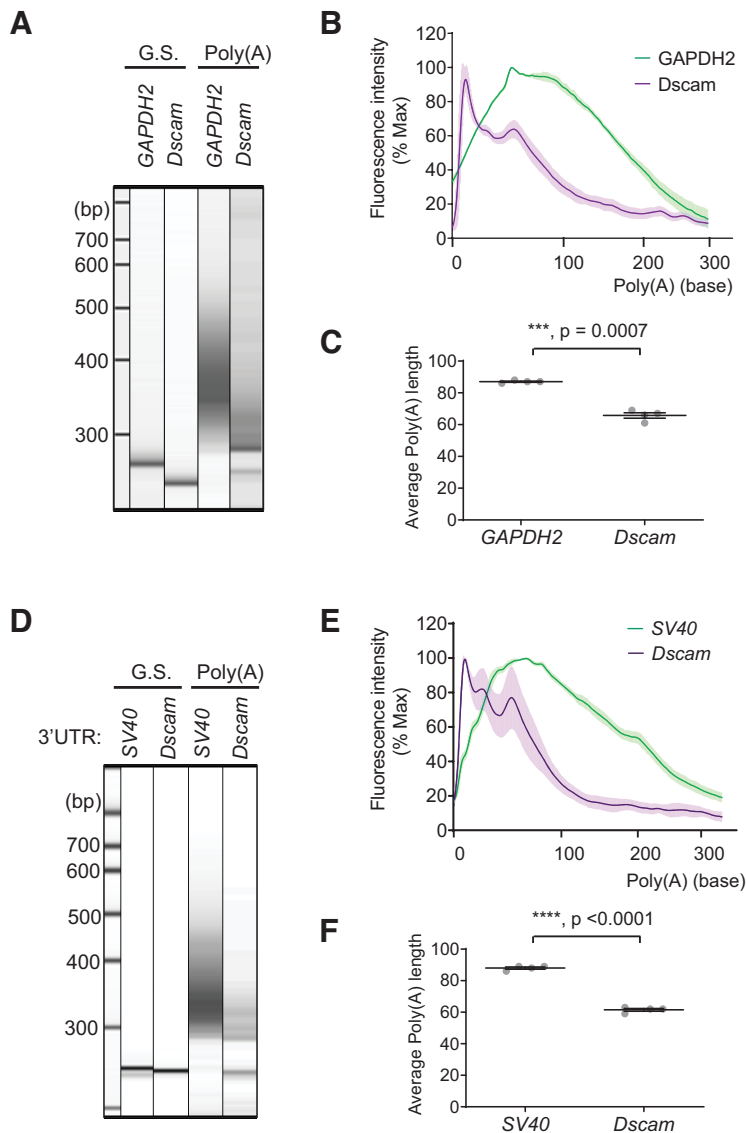


Figure 5. *Dscam* mRNA contains short poly(A) tails. **A**, Total RNA was extracted from the third instar larva brains from a wild-type control (w^{1118}) and subjected to the poly(A) length analysis. Capillary gel electrophoresis images were shown for the gene-specific (G.S.) PCR product as a discrete band (the first and second lane) for *GAPDH2* and *Dscam*. The PCR product using universal reverse primer exhibits a smear pattern (the third and fourth lane), which indicates the mRNAs with a range of poly(A) tail. **B**, The poly(A) length from *GAPDH2* (green) and *Dscam* (magenta) was calculated from the capillary gel electrophoresis (see above, Materials and Methods), and the distribution was plotted from four technical replicates (mean \pm SD). Note a difference in peak poly(A) length. **C**, Mean poly(A)-tail lengths were calculated and are displayed (mean \pm SEM, $t = 12.14$, $df = 3.344$, $p = 0.0007$, 2-tailed Welch's t test; sample $n = 4$). **D**, *Drosophila* S2 cells were cotransfected with the *Dscam* constructs that contain *Dscam*-5' UTR, the coding region of *Dscam*, and the 3' UTR of either *Dscam* or *SV40* and subjected to the poly(A) length analysis. Capillary gel electrophoresis images were shown for the gene-specific (G.S.) PCR product as a discrete band (the first and second lane) for *Dscam*-5' UTR-*Dscam*-3' UTR (*SV40*) and *Dscam*-5' UTR-*Dscam*-3' UTR (*Dscam*). The PCR product using universal reverse primer exhibits a smear pattern (the third and fourth lane), which indicates the mRNAs with a range of poly(A) tail. **E**, The poly(A) length from *Dscam*-5' UTR-*Dscam*-3' UTR (*SV40*, green) and *Dscam*-5' UTR-*Dscam*-3' UTR (*Dscam*, magenta) was calculated from the capillary gel electrophoresis, and the distribution was plotted from four technical replicates (mean \pm SD). **F**, Mean poly(A)-tail lengths were calculated and displayed (mean \pm SEM, $t = 23.70$, $df = 5.769$, $p < 0.0001$, 2-tailed Welch's t test; sample $n = 4$ *** $p < 0.001$ and **** $p < 0.0001$).

pAbp^{K10109/EP310} (Fig. 4B). Thus, pAbp proteins are not expressed in excess and can be a limiting factor for general translation initiation. This indicates that *Dscam* translation is more sensitive to a reduction in pAbp protein levels than other canonical targets.

This relative sensitivity suggests that *Dscam* mRNA may not provide a high-affinity binding site as other cellular mRNAs via

poly(A) tail. Certain mRNAs undergo a process known as the cytoplasmic deadenylation, a form of post-transcriptional translational regulation (Richter, 1999). Interestingly, some isoforms of mouse *Dscam* mRNAs reportedly contain very short poly(A) tails of only 5–10 adenine residues (Alves-Sampaio et al., 2010). Efficient PABP-C recruitment to a poly(A) tail requires ~ 27 adenine nucleotides (Deo et al., 1999). Thus, we decided to measure the lengths of the poly(A) tails of *Dscam* mRNA. To this end, we used a poly(A) tail analysis known as the G/I tailing (Kusov et al., 2001). To measure the poly(A) lengths of *Dscam*, total RNA was extracted from the larval brains from a wild-type control (w^{1118}) and subjected to the poly(A) length analysis. *GAPDH2* was used as a control. Polyadenylation is not a defined modification; therefore, the PCR product generates a smear pattern (Fig. 5A). The identity of the smear PCR band from *GAPDH2* and *Dscam* were verified by sequencing.

The sizes of poly(A) PCR products and the gene-specific PCR product were used to calculate the poly(A) tail lengths of the gene of interest (Fig. 5B; see above, Materials and Methods). The result showed that *Dscam* has significantly shorter poly(A) tails than those from *GAPDH2* (Fig. 5C). Unlike a bell-shape distribution of *GAPDH2* poly(A) tails, *Dscam* poly(A) tails showed a sharp peak. The peak poly(A) tail length of *Dscam* was 5.75 ± 2.36 bases compared with 47.25 ± 1.26 bases of *GAPDH2* (Fig. 5B). Wnd regulation on *Dscam* expression requires *Dscam*-3' UTR (Fig. 3). Therefore, we wondered whether the short poly(A) tails of *Dscam* mRNA is dependent on *Dscam*-3' UTR. We coexpressed the *Dscam* DNA constructs that contains either *SV40*-3' UTR or *Dscam*-3' UTR in *Drosophila* S2 cells. Total RNA was prepared from the S2 cell lysates and subjected to subsequent poly(A) length analysis. The result showed that the poly(A) tail distributions from *Dscam*-*SV40*-3' UTR were almost identical as those from *GAPDH2*, whereas those from *Dscam*-*Dscam*-3' UTR showed a similar pattern as those from endogenous *Dscam* (Fig. 5B,C,E,F). This clearly demonstrates that *Dscam* mRNAs contain short poly(A) tails, which is dependent on *Dscam*-3' UTR and further suggests a presence of pAbp binding site outside the poly(A) tail of *Dscam* mRNA.

pAbp Physically interacts with an adenine-rich region in the *Dscam* 3' UTR

Interestingly, PABP can interact with RNA sequences outside of poly(A) tail but rich in adenine nucleotides (Skabkina et al., 2003; Sladic et al., 2004; Vazquez-Pianzola et al., 2011; Kini et al., 2016; Smith et al., 2017). We reasoned that such binding likely takes place in the 3' UTR of *Dscam* because Wnd regulation of *Dscam* requires it. To test the possibility that the *Dscam*-3' UTR contains pAbp binding sites, bioinformatic analysis was performed using an RBP binding prediction tool (Paz et al., 2014). We selected the motifs that are shared by both *Drosophila* pAbp and human PABP-C1. The

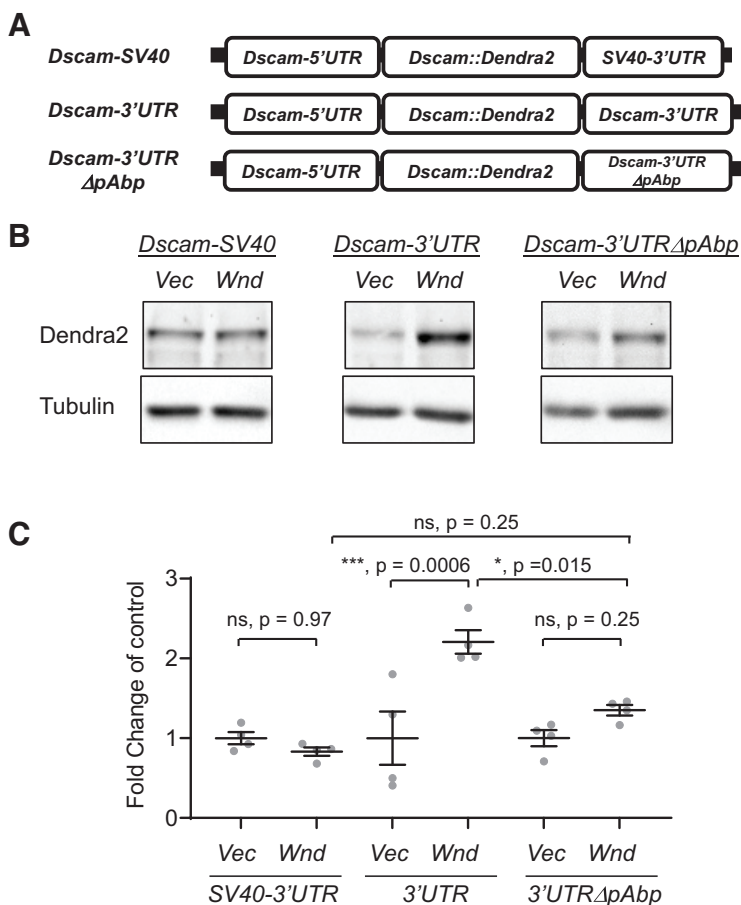


Figure 7. *pAbp* binding to *Dscam*-3'UTR is required for Wnd-induced *Dscam* translation in S2 cells. **A**, Schematics of *Dscam*-5'UTR-*Dscam*::*Dendra2*-*SV40*-3'UTR (*5-Dscam-SV40*), *Dscam*-5'UTR-*Dscam*::*Dendra2*-*Dscam*-3'UTR (*5-Dscam-3UTR*), and *Dscam*-5'UTR-*Dscam*::*Dendra2*-*Dscam*-3'UTRΔ*pAbp* (*5-Dscam-3UTRΔpAbp*) are shown. All *Dscam*-3'UTR DNA constructs contains endogenous PAS from *Dscam*. **B**, S2 cells were transfected with indicated *Dscam* constructs along with either an empty vector (*Vec*) or Wnd-expressing construct. Total cell lysates were subjected to Western blot analysis using anti-*Dendra2* antibody to detect *Dscam*::*Dendra2*. Tubulin blot was used as a loading control. A representative image from four replicate experiments is shown. **C**, *Dendra2* blots were normalized with tubulin blot and expressed as a fold change of a corresponding control (Wnd/*Vec*) from *Dscam*-*SV40*, *Dscam*-3'UTR, and *Dscam*-3'UTRΔ*pAbp*. The data were expressed as mean \pm SEM; one-way ANOVA ($F_{(5,18)} = 9.899$, $p = 0.0001$) followed by *post hoc* Tukey's multiple comparison test. The *p* values from Tukey's test are indicated in the graph; sample $n = 4$ * $p < 0.05$, *** $p < 0.001$, and ns = not significant.

(*Dscam*-Δ*pAbp*; Fig. 6A). The RNAs were incubated with S2 cell lysates. Bound *pAbp* was detected using Western blot analysis (Fig. 6B) following the quantitation of either using *SV40* or *Dscam*-Δ*pAbp* as a control (Fig. 6C). In either quantitation, *Dscam* region showed an increased *pAbp*-binding (~2.5-fold) than the controls. The specificity of the *pAbp* antibody was verified using the S2 cell lysates that were treated with *pAbp* dsRNA (Fig. 6D). These results demonstrate that *pAbp* physically interacts with *Dscam*-3'UTR, which is dependent on the 123-nucleotide A-rich region.

The interaction between *pAbp* and *Dscam* 3'UTR mediates Wnd-induced increase in *dscam* expression

Next, we determined whether this noncanonical interaction of *pAbp* with *Dscam* mRNA is required for Wnd-mediated *Dscam* upregulation. We generated *Dscam*-expressing DNA constructs that contain *SV40*-3'UTR, *Dscam*-3'UTR, or a *Dscam*-3'UTR without the A-rich region (*Dscam*-3'UTRΔ*pAbp*; Fig. 7A). The transgenic *Dscam* proteins were tagged with the fluorescent

protein *Dendra2*. We coexpressed a Wnd construct along with the *Dscam* constructs in S2 cells. Western blot analysis showed that although Wnd dramatically increased the expression of *Dscam* from *Dscam*::*Dendra2*-*Dscam*-3'UTR, it only mildly increased *Dscam* expression from *Dscam*::*Dendra2*-*Dscam*-3'UTRΔ*pAbp* (Fig. 7B, C). There was about a one-fold difference in Wnd-induced *Dscam* increase between *Dscam*::*Dendra2*-*Dscam*-3'UTR and *Dscam*::*Dendra2*-*Dscam*-3'UTRΔ*pAbp* (Fig. 7C). Next, we tested whether the A-rich region is sufficient to confer Wnd-mediated upregulation. We inserted the A-rich region from *Dscam*-3'UTR in *SV40*-3'UTR just before the PAS (Fig. 8, top). *Dscam* was expressed under the modified *SV40*-3'UTR (A-rich-*SV40*) in the presence of Wnd in S2 cells. We found no changes in *Dscam* expression (Fig. 8), which suggests the presence of an A-rich region per se is not sufficient for Wnd-mediated regulation.

To determine whether the interaction between *pAbp* and *Dscam* 3'UTR is essential for *Dscam* expression *in vivo*, we expressed the *Dscam* transgenes in *Drosophila* C4da neurons using a *ppk*-*GAL4* driver in wild-type and *highwire* (*hiw*) mutants. We found that loss of *hiw* increased the expression of *Dscam* from *Dscam*::*Dendra2*-*Dscam*-3'UTR, but not that from *Dscam*::*Dendra2*-*SV40*-3'UTR (Fig. 9). Consistent with our *in vitro* result (Fig. 7B,C), loss of *hiw* caused a significantly smaller increase in *Dscam* expression from *Dscam*::*Dendra2*-*Dscam*-3'UTRΔ*pAbp* than from *Dscam*::*Dendra2*-*Dscam*-3'UTR (Fig. 9B). These results demonstrate that the interaction between *pAbp* and *Dscam*-3'UTR is essential for Wnd-induced enhancement of *Dscam* expression.

Discussion

DLK plays essential roles in multiple biological processes in the nervous system, some of which require post-transcriptional regulations of molecules in the DLK pathway. One of the molecules downstream of DLK is *Dscam*, whose altered expression is associated with multiple brain disorders. In this study, we identified *pAbp*, the *Drosophila* ortholog of PABP-C, as an RBP that mediates Wnd-induced post-transcriptional upregulation of *Dscam*. Our study revealed that the noncanonical recruitment of PABP-C to the 3'UTR of *Dscam* is essential in the process. Thus, our study uncovers a novel mechanism of DLK-mediated post-transcriptional gene regulation.

We showed that *pAbp* is required for Wnd-induced *Dscam* upregulation (Figs. 1, 3) as well as Wnd-induced increase in pre-synaptic arbor size (Fig. 2). How does *pAbp*, as a general mRNA translation activator, affect *Dscam* expression? It is known that simultaneous interaction between PABP-C and poly(A) tails and that between PABP-C and the mRNA translation initiation complex at the 5'-end of an mRNA underlies the role of PABP-C in the activation of mRNA translation (Munroe and Jacobson, 1990; Wells et al., 1998). However, recent studies have shown that PABP-C also can exert mRNA-specific post-transcriptional regulation through interacting the 5' or 3'UTR of target mRNAs (Wu and Bag, 1998; Lyabin et al., 2011; Eliseeva et al., 2012;

Iwakawa et al., 2012; Casper et al., 2013; Smith et al., 2017). These interactions lead to either a suppression or an activation of target translation, depending on target mRNA. In a conventional model, PABP-C bridges the 3'- and 5'-end of an mRNA for generating a closed-loop structure for efficient mRNA translation (Munroe and Jacobson, 1990; Wells et al., 1998). Interestingly, the recruitment of PABP-C to the 3'UTR of target mRNAs leads to translational activation (Lyabin et al., 2011; Eliseeva et al., 2012; Iwakawa et al., 2012; Smith et al., 2017). Consistently, our result strongly suggests that *Dscam*-3'UTR contains an A-rich region, which can recruit pAbp (Fig. 6). These suggest that the noncanonical PABP-C association near the end of 3'-UTR may involve a similar mechanism as the closed-loop model for translational activation.

Our result showed that *pAbp* knock-down selectively suppressed Wnd-induced upregulation of *Dscam*-3'UTR reporter but not that of SV40-3'UTR reporter or Wnd expression (Fig. 1). PABP controls general protein synthesis. How does *pAbp* RNAi selectively affect *Dscam* translation? PABP has a strong binding affinity toward the poly(A) tail and shows significantly lower affinity toward nonpoly(A) RNA sequences (Sladic et al., 2004). Our result indicates that *Drosophila Dscam* mRNAs have short poly(A) tails (Fig. 5), which is consistent with a previous report in mouse *Dscam* (Alves-Sampaio et al., 2010). Given that efficient PABP-C recruitment requires ~27 consecutive adenine nucleotides (Deo et al., 1999), the absence of strong PABP-C binding through a poly(A) tail likely renders *Dscam* mRNA more dependent on the A-rich region in its 3'UTR. In this scenario, the noncanonical PABP binding requires a higher PABP concentration than that of canonical poly(A) tail interaction, which would make noncanonical interaction more sensitive to a reduction in cytoplasmic PABP protein levels. PABP is known to regulate its own protein homeostasis through binding its own 5'UTR and translational suppression (Wu and Bag, 1998). This autoregulation might not be as strong as it is believed as our analysis of transheterozygous *pAbp* mutants showed ~50% reduction in general mRNA translation (Fig. 4). Nevertheless, our result showed that *pAbp* mutations caused more notable suppression of *Dscam* expression compared with that of a mCD8::RFP, a normalizing experimental control that contains SV40-3'UTR (Fig. 3). To further rule out a possibility of general mRNA translation suppression by *pAbp* mutations, we used Wnd-HSL in our study (Figs. 2B, 3). The translation of histone mRNAs employs a unique mechanism because these are the only metazoan mRNAs that do not possess poly(A) tails. The HSL at the 3'-end of histone mRNA recruits SLBP instead of PABP, which promotes the translation initiation of histone mRNA (Ling et al., 2002; Sánchez and Marzluff, 2002). Together, we envision that pAbp exerts a relative selectivity toward *Dscam* translation via a differential affinity toward canonical and noncanonical RNA interactions.

Our study shows that Wnd requires pAbp for enhancing *Dscam* expression (Figs. 1, 3) and for increasing presynaptic arbor growth (Fig. 2). This suggests that Wnd/DLK regulates PABP activity. Wnd is an upstream kinase in the MAP kinase

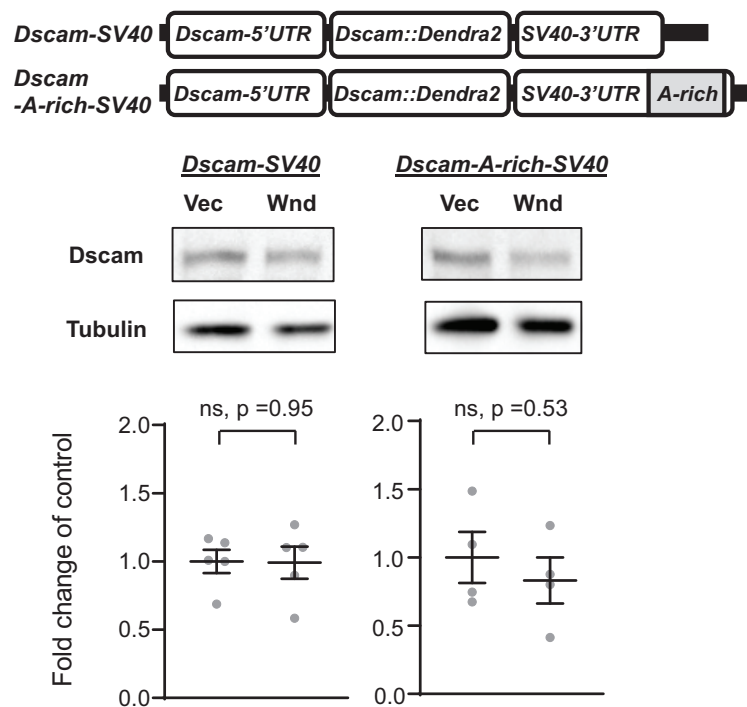


Figure 8. The A-rich region of *Dscam* is not sufficient for Wnd regulation. The 123-bp A-rich sequence from *Dscam*-3'UTR was inserted at the 148 bp upstream of the polyadenylation signal in *Dscam*-5'UTR-*Dscam*::*Dendra2*-SV40-3'UTR (*Dscam*-A-rich-SV40) (top) and expressed in *Drosophila* S2 cells in the presence of an empty vector (Vec) or Wnd expressing plasmid. Total lysates were subjected to Western blot with anti-*Dendra2* to quantify *Dscam*::*Dendra2* (*Dscam*). Tubulin blot was used as a loading control. The expression of *Dscam*-5'UTR-*Dscam*::*Dendra2*-SV40-3'UTR (*Dscam*-SV40) was shown as a comparison. The data were expressed as mean \pm SEM. The two-tailed Welch's *t* test ($t = 0.06, 013$, $df = 7.289$ for *Dscam*-SV40 and $t = 0.6723$, $df = 5.937$ for *Dscam*-A-rich-SV40); sample $n = 5$; *ns = not significant.

pathway. It is possible that Wnd or downstream MAP kinases phosphorylate PABP and modify PABP affinity toward the non-canonical A-rich sequence in *Dscam*-3'UTR. For example, PABP is phosphorylated by CRK1, which promotes association with the poly(A) sequence, self-interaction, and interaction with eIF4E in *Trypanosoma brucei* (An et al., 2018). However, although human PABP-C is highly modified post-translationally via methylation and acetylation (Brook et al., 2012), PABP-C phosphorylation has not been detected in most animals. Then, how might Wnd modify PABP activity? Interestingly, A-rich sequences are not rare in the UTR sequences. In fact, the SV40-3'UTR segment that was used in our study (Fig. 6) also contains four putative noncanonical PABP binding sites, although it did not show a specific pAbp binding (Fig. 6) or being regulated by Wnd expression or a loss of *hiw* (Figs. 3, 7, 9). This raises an interesting possibility that these A-rich sequences may require additional factors for recruiting PABP-C. Consistent with this idea, inserting the A-rich region from *Dscam*-3'UTR in SV40-3'UTR did not affect reporter expression in the presence of Wnd (Fig. 8). The DLK/Wnd pathway may phosphorylate an unknown cofactor, which increases PABP-C recruitment to the A-rich region in the target 3'UTR. RNAi is known to have false negatives (Booker et al., 2011). Our RNAi screen may have simply missed the cofactor. It will be important to identify this cofactor to gain a complete understanding of DLK signaling in future studies.

Although our analyses showed that pAbp is critically required for Wnd-mediated presynaptic arborization (Fig. 2B) and *Dscam* expression (Fig. 3), the hypomorphic mutant *pAbp*^{K10109/EP310} showed only a mild effect in presynaptic arborization by *hiw* mutations (Fig. 2A). Complete loss of *pAbp* triggers cell lethality

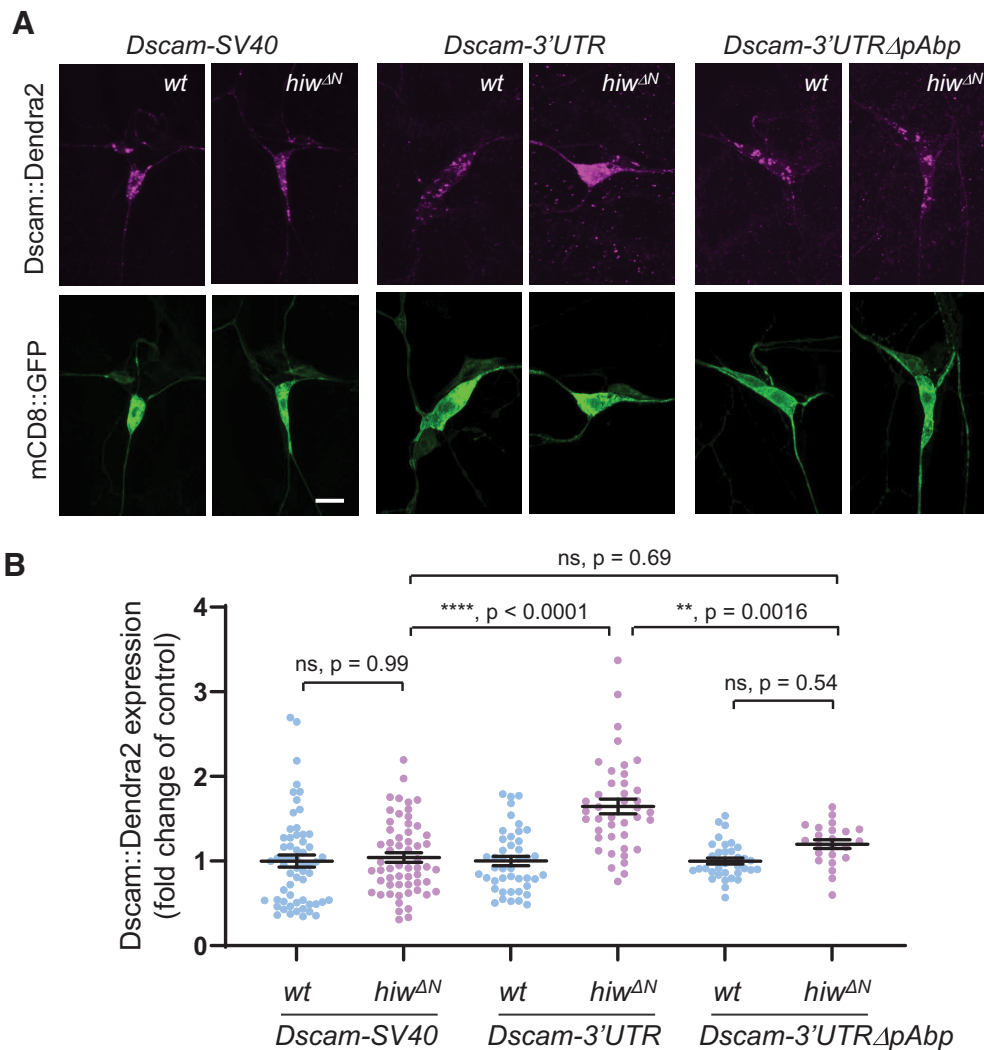


Figure 9. *pAbp* binding to *Dscam*-3' UTR is required for Wnd-induced *Dscam* translation *in vivo*. **A**, The *Dscam*::*Dendra2* transgenes, *Dscam*-5' UTR-*Dscam*::*Dendra2*-*SV40*-3' UTR (*Dscam*-*SV40*), *Dscam*-5' UTR-*Dscam*::*Dendra2*-*Dscam*-3' UTR (*Dscam*-3' UTR), and *Dscam*-5' UTR-*Dscam*::*Dendra2*-*Dscam*-3' UTRΔ*pAbp* (*Dscam*-3' UTRΔ*pAbp*) were expressed in C4da neurons with *ppk*-*GAL4* either in wild-type control (w^{1118} , wt) or in *hiw* mutant ($hiw^{\Delta N}$) animals. The expression levels of *Dscam*::*Dendra2* were measured from the individual C4da cell bodies. *Dscam*::*Dendra2* expression levels were visualized with anti-*Dendra2* antibody (magenta). A membrane marker, *mCD8*::*GFP*, was used as a normalizing control (green). Hemizygous male *hiw* mutant ($hiw^{\Delta N}$) and male wild-type (w^{1118}) animals were used. Scale bar, 10 μ m. **B**, *Dscam*::*Dendra2* fluorescence intensity was normalized by *mCD8*::*GFP* fluorescence intensity and expressed as a fold change of a corresponding control ($hiw^{\Delta N}/wt$) from *Dscam*-5' UTR-*Dscam*::*Dendra2*-*SV40*-3' UTR (*Dscam*-*SV40*), *Dscam*-5' UTR-*Dscam*::*Dendra2*-*Dscam*-3' UTR (*Dscam*-3' UTR), and *Dscam*-5' UTR-*Dscam*::*Dendra2*-*Dscam*-3' UTRΔ*pAbp* (*Dscam*-3' UTRΔ*pAbp*). The data were expressed as median \pm 95% CI. One-way ANOVA ($F_{(5,255)} = 14.40$, $p < 0.0001$) followed by *post hoc* Tukey's multiple comparison test. The *p* values from Tukey's test are indicated in the graph. Sample numbers were *Dscam*-*SV40* in wt (w^{1118} ; *UAS*-*Dscam*-5' UTR-*Dscam*::*Dendra2*-*SV40*-3' UTR/+; *ppk*-*GAL4*, *UAS*-*mCD8*::*GFP*/+) ($n = 60$), *Dscam*-*SV40* in $hiw^{\Delta N}$ ($hiw^{\Delta N}$; *UAS*-*Dscam*-5' UTR-*Dscam*::*Dendra2*-*SV40*-3' UTR/+; *ppk*-*GAL4*, *UAS*-*mCD8*::*GFP*/+) ($n = 58$), *Dscam*-3' UTR in wt (w^{1118} ; *UAS*-*Dscam*-5' UTR-*Dscam*::*Dendra2*-*Dscam*-3' UTR/+; *ppk*-*GAL4*, *UAS*-*mCD8*::*GFP*/+) ($n = 44$), *Dscam*-3' UTR in $hiw^{\Delta N}$ ($hiw^{\Delta N}$; *UAS*-*Dscam*-5' UTR-*Dscam*::*Dendra2*-*Dscam*-3' UTR/+; *ppk*-*GAL4*, *UAS*-*mCD8*::*GFP*/+) ($n = 41$), *Dscam*-3' UTRΔ*pAbp* in wt (w^{1118} ; *UAS*-*Dscam*-5' UTR-*Dscam*::*Dendra2*-*Dscam*-3' UTRΔ*pAbp*/+; *ppk*-*GAL4*, *UAS*-*mCD8*::*GFP*/+) ($n = 35$), and *Dscam*-3' UTRΔ*pAbp* in $hiw^{\Delta N}$ ($hiw^{\Delta N}$; *UAS*-*Dscam*-5' UTR-*Dscam*::*Dendra2*-*Dscam*-3' UTRΔ*pAbp*/+; *ppk*-*GAL4*, *UAS*-*mCD8*::*GFP*/+) ($n = 23$) ** $p < 0.01$, **** $p < 0.0001$, and ns = not significant.

because *pAbp* is required for general protein synthesis. We estimate that $\sim 50\%$ of *pAbp* function is lost in *pAbp*^{K10109/EP310} (Fig. 4), which may explain a partial rescue in *hiw*-induced axon arborization. Wnd-enhanced *Dscam* expression was reduced by $\sim 61\%$ in *pAbp*^{K10109/EP310} mutants (Fig. 3B). Conversely, this may suggest that *Hiw* uses additional, Wnd-independent pathway for axonal arborization in C4da neurons. Consistently, $\sim 30\%$ of *hiw*-enhanced *Dscam* expression remained in *Dscam*::*Dendra2*-*Dscam*-3' UTRΔ*pAbp* (Fig. 9B). Although statistically insignificant, deleting the A-rich region from *Dscam*-3' UTR did not completely abolish Wnd-enhanced *Dscam* expression both in S2 cells and C4da neurons (Figs. 7, 9). Thus, this may suggest an existence of an independent RBP pathway downstream of Wnd in *Dscam* expression regulation.

Many functions of DLK are conserved from worms to mice, some of which rely on post-transcriptional gene regulation. Here, we show that the *Drosophila* ortholog of PABP-C is involved in presynaptic arbor growth through mediating post-transcriptional regulation of *Dscam*. The DLK homolog in *C. elegans* promotes mRNA stability of *CEBP* in response to axonal injury (Yan et al., 2009). A noncanonical PABP-C interaction is known for mRNA stability and localization of *osk* mRNA in *Drosophila* (Vazquez-Pianzola et al., 2011). Thus, it is conceivable that PABP-C may mediate multiple DLK functions. Interestingly, recent studies suggest a novel role of DLK and PABP-C in neuropathic pain (Barragán-Iglesias et al., 2018; Wlaschin et al., 2018; Hu et al., 2019; Ma et al., 2021). It is possible that DLK and PABP-C target the same set of mRNAs in

neuropathic pain. What factors or features would make these mRNAs under DLK-PABP control? Our results showed that *Dscam*-3'UTR has an A-rich region for direct pAbp recruitment (Fig. 6). In addition, *Dscam* mRNA has short poly(A) tails, which are dependent on *Dscam*-3'UTR (Fig. 5). The length of poly(A) tails is under the control of multiple pathways (Richter, 1999; Meijer et al., 2007; Nicholson and Pasquinelli, 2019). These may be the common features of DLK-PABP-targeted mRNAs. DLK is expressed in nonneuronal cell types and may function in these cell types (Jin and Zheng, 2019). Determining the roles of PABP-C and common mRNA targets downstream of various DLK functions will be an important research direction for future studies.

References

- Akiyoshi Y, Clayton J, Phan L, Yamamoto M, Hinnebusch AG, Watanabe Y, Asano K (2001) Fission yeast homolog of murine Int-6 protein, encoded by mouse mammary tumor virus integration site, is associated with the conserved core subunits of eukaryotic translation initiation factor 3. *J Biol Chem* 276:10056–10062.
- Alavi M, Song M, King GLA, Gillis T, Propst R, Lamanuzzi M, Bousum A, Miller A, Allen R, Kidd T (2016) *Dscam1* forms a complex with Robo1 and the N-terminal fragment of slit to promote the growth of longitudinal axons. *PLoS Biol* 14:e1002560.
- Alves-Sampaio A, Troca-Marin JA, Montesinos ML (2010) NMDA-mediated regulation of DSCAM dendritic local translation is lost in a mouse model of Down's syndrome. *J Neurosci* 30:13537–13548.
- Amano K, Yamada K, Iwayama Y, Detera-Wadleigh SD, Hattori E, Toyota T, Tokunaga K, Yoshikawa T, Yamakawa K (2008) Association study between the Down syndrome cell adhesion molecule (DSCAM) gene and bipolar disorder. *Psychiatr Genet* 18:1–10.
- An T, Liu Y, Gourguechon S, Wang CC, Li Z (2018) CDK phosphorylation of translation initiation factors couples protein translation with cell-cycle transition. *Cell Rep* 25:3204–3214.
- Antic S, Wolfinger MT, Skucha A, Hosiner S, Dorner S (2015) General and microRNA-mediated mRNA degradation occurs on ribosome complexes in *Drosophila* cells. *Mol Cell Biol* 35:2309–2320.
- Barragán-Iglesias P, Lou TF, Bhat VD, Megat S, Burton MD, Price TJ, Campbell ZT (2018) Inhibition of Poly(A)-binding protein with a synthetic RNA mimic reduces pain sensitization in mice. *Nat Commun* 9:10.
- Bischof J, Maeda RK, Hediger M, Karch F, Basler K (2007) An optimized transgenesis system for *Drosophila* using germ-line-specific phiC31 integrases. *Proc Natl Acad Sci U S A* 104:3312–3317.
- Blondeau A, Lucier J-F, Matteau D, Dumont L, Rodrigue S, Jacques P-É, Blouin R (2016) Dual leucine zipper kinase regulates expression of axon guidance genes in mouse neuronal cells. *Neural Dev* 11:13.
- Booker M, Samsonova AA, Kwon Y, Flockhart I, Mohr SE, Perrimon N (2011) False negative rates in *Drosophila* cell-based RNAi screens: a case study. *BMC Genomics* 12:50.
- Brook M, McCracken L, Reddington JP, Lu ZL, Morrice NA, Gray NK (2012) The multifunctional poly(A)-binding protein (PABP) 1 is subject to extensive dynamic post-translational modification, which molecular modelling suggests plays an important role in co-ordinating its activities. *Biochem J* 441:803–812.
- Bruce FM, Brown S, Smith JN, Fuerst PG, Erskine L (2017) DSCAM promotes axon fasciculation and growth in the developing optic pathway. *Proc Natl Acad Sci U S A* 114:1702–1707.
- Casper I, Nowag S, Koch K, Hubrich T, Bollmann F, Henke J, Schmitz K, Kleinert H, Pautz A (2013) Post-transcriptional regulation of the human inducible nitric oxide synthase (iNOS) expression by the cytosolic poly(A)-binding protein (PABP). *Nitric Oxide* 33:6–17.
- Collins CA, Wairkar YP, Johnson SL, DiAntonio A (2006) Highwire restrains synaptic growth by attenuating a MAP kinase signal. *Neuron* 51:57–69.
- Deo RC, Bonanno JB, Sonenberg N, Burley SK (1999) Recognition of polyadenylated RNA by the poly(A)-binding protein. *Cell* 98:835–845.
- Eggers DK, Welch WJ, Hansen WJ (1997) Complexes between nascent polypeptides and their molecular chaperones in the cytosol of mammalian cells. *Mol Biol Cell* 8:1559–1573.
- Eliseeva IA, Ovchinnikov LP, Lyabin DN (2012) Specific PABP effect on translation of YB-1 mRNA is neutralized by polyadenylation through a “mini-loop” at 3' UTR. *RNA Biol* 9:1473–1487.
- Fuerst PG, Koizumi A, Masland RH, Burgess RW (2008) Neurite arborization and mosaic spacing in the mouse retina require DSCAM. *Nature* 451:470–474.
- Fuerst PG, Bruce F, Tian M, Wei W, Elstrott J, Feller MB, Erskine L, Singer JH, Burgess RW (2009) DSCAM and DSCAML1 function in self-avoidance in multiple cell types in the developing mouse retina. *Neuron* 64:484–497.
- Ghosh AS, Wang B, Pozniak CD, Chen M, Watts RJ, Lewcock JW (2011) DLK induces developmental neuronal degeneration via selective regulation of proapoptotic JNK activity. *J Cell Biol* 194:751–764.
- Grueber WB, Ye B, Yang C-H, Younger S, Borden K, Jan LY, Jan Y-N (2007) Projections of *Drosophila* multidendritic neurons in the central nervous system: links with peripheral dendrite morphology. *Development* 134:55–64.
- Harel-Sharvit L, Eldad N, Haimovich G, Barkai O, Duek L, Choder M (2010) RNA polymerase II subunits link transcription and mRNA decay to translation. *Cell* 143:552–563.
- Hu Z, Deng N, Liu K, Zeng W (2019) DLK mediates the neuronal intrinsic immune response and regulates glial reaction and neuropathic pain. *Exp Neurol* 322:1–13.
- Iwakawa H-o, Tajima Y, Taniguchi T, Kaido M, Mise K, Tomari Y, Taniguchi H, Okuno T (2012) Poly(A)-binding protein facilitates translation of an uncapped/nonpolyadenylated viral RNA by binding to the 3' untranslated region. *J Virol* 86:7836–7849.
- Jin Y, Zheng B (2019) Multitasking: dual leucine zipper-bearing kinases in neuronal development and stress management. *Annu Rev Cell Dev Biol* 35:501–521.
- Kim JH, Wang X, Coolon R, Ye B (2013) Dscam expression levels determine presynaptic arbor sizes in drosophila sensory neurons. *Neuron* 78:827–838.
- Kini HK, Silverman IM, Ji X, Gregory BD, Liebhaber SA (2016) Cytoplasmic poly(A) binding protein-1 binds to genomically encoded sequences within mammalian mRNAs. *RNA* 22:61–74.
- Klinedinst S, Wang X, Xiong X, Haeflner JM, Collins CA (2013) Independent pathways downstream of the Wnd/DLK MAPKKK regulate synaptic structure, axonal transport, and injury signaling. *J Neurosci* 33:12764–12778.
- Kusov YY, Shatirishvili G, Dzagurov G, Gauss-Müller V (2001) A new G-tailing method for the determination of the poly(A) tail length applied to hepatitis A virus RNA. *Nucleic Acids Res* 29:e57-7.
- Larhammar M, Huntwork-Rodriguez S, Jiang Z, Solanoy H, Ghosh AS, Wang B, Kaminker JS, Huang K, Eastham-Anderson J, Siu M, Modrusan Z, Farley MM, Tessier-Lavigne M, Lewcock JW, Watkins TA (2017) Dual leucine zipper kinase-dependent PERK activation contributes to neuronal degeneration following insult. *Elife* 6:e20725.
- Le Pichon CE, et al. (2017) Loss of dual leucine zipper kinase signaling is protective in animal models of neurodegenerative disease. *Sci Transl Med* 9:eaag0394.
- Lee T, Luo L (2001) Mosaic analysis with a repressible cell marker (MARCM) for *Drosophila* neural development. *Trends Neurosci* 24:251–254.
- Ling J, Morley SJ, Pain VM, Marzluff WF, Gallie DR (2002) The histone 3'-terminal stem-loop-binding protein enhances translation through a functional and physical interaction with eukaryotic initiation factor 4G (eIF4G) and eIF3. *Mol Cell Biol* 22:7853–7867.
- Lyabin DN, Eliseeva IA, Skabkina OV, Ovchinnikov LP (2011) Interplay between Y-box-binding protein 1 (YB-1) and poly(A) binding protein (PABP) in specific regulation of YB-1 mRNA translation. *RNA Biol* 8:883–892.
- Ma J, Goodwani S, Acton PJ, Buggia-Prevot V, Kesler SR, Jamal I, Mahant ID, Liu Z, Mseeh F, Roth BL, Chakraborty C, Peng B, Wu Q, Jiang Y, Le K, Soth MJ, Jones P, Kavelaars A, Ray WJ, Heijnen CJ (2021) Inhibition of dual leucine zipper kinase prevents chemotherapy-induced peripheral neuropathy and cognitive impairments. *Pain* 162:2599–2612.
- Marzluff WF, Wagner EJ, Duronio RJ (2008) Metabolism and regulation of canonical histone mRNAs: life without a poly(A) tail. *Nat Rev Genet* 9:843–854.
- Meijer HA, Bushell M, Hill K, Gant TW, Willis AE, Jones P, de Moor CH (2007) A novel method for poly(A) fractionation reveals a large population of mRNAs with a short poly(A) tail in mammalian cells. *Nucleic Acids Res* 35:e132.

- Mohr SE, Hu Y, Rudd K, Buckner M, Gilly Q, Foster B, Sierzputowska K, Comjean A, Ye B, Perrimon N (2015) Reagent and data resources for investigation of RNA binding protein functions in *Drosophila melanogaster* cultured cells. *G3 (Bethesda)* 5:1919–1924.
- Munroe D, Jacobson A (1990) mRNA poly(A) tail, a 3' enhancer of translational initiation. *Mol Cell Biol* 10:3441–3455.
- Nakata K, Abrams B, Grill B, Goncharov A, Huang X, Chisholm AD, Jin Y (2005) Regulation of a DLK-1 and p38 MAP kinase pathway by the ubiquitin ligase RPM-1 is required for presynaptic development. *Cell* 120:407–420.
- Nicholson AL, Pasquinelli AE (2019) Tales of detailed poly(A) tails. *Trends Cell Biol* 29:191–200.
- O'Roak BJ, Stessman HA, Boyle EA, Witherspoon KT, Martin B, Lee C, Vives L, Baker C, Hiatt JB, Nickerson DA, Bernier R, Shendure J, Eichler EE (2014) Recurrent *de novo* mutations implicate novel genes underlying simplex autism risk. *Nat Commun* 5:5595.
- Paz I, Kosti I, Ares M, Cline M, Mandel-Gutfreund Y (2014) RBPmap: a Web server for mapping binding sites of RNA-binding proteins. *Nucleic Acids Res* 42:W361–W367.
- Pestka S (1971) Inhibitors of ribosome functions. *Annu Rev Microbiol* 25:487–562.
- Richter JD (1999) Cytoplasmic polyadenylation in development and beyond. *Microbiol Mol Biol Rev* 63:446–456.
- Sánchez R, Marzluff WF (2002) The stem-loop binding protein is required for efficient translation of histone mRNA *in vivo* and *in vitro*. *Mol Cell Biol* 22:7093–7104.
- Santos RA, Fuertes AJC, Short G, Donohue KC, Shao H, Quintanilla J, Malakzadeh P, Cohen-Cory S (2018) DSCAM differentially modulates pre- and postsynaptic structural and functional central connectivity during visual system wiring. *Neural Dev* 13:22.
- Schmucker D, Chen B (2009) Dscam and DSCAM: complex genes in simple animals, complex animals yet simple genes. *Genes Dev* 23:147–156.
- Schramm RD, Li S, Harris BS, Rounds RP, Burgess RW, Ytreberg FM, Fuerst PG (2012) A novel mouse Dscam mutation inhibits localization and shedding of DSCAM. *PLoS One* 7:e52652.
- Shen L, Xiao Z, Pan Y, Fang M, Li C, Chen D, Wang L, Xi Z, Xiao F, Wang X (2011) Altered expression of Dscam in temporal lobe tissue from human and experimental animals. *Synapse* 65:975–982.
- Shin JE, Cho Y, Beirowski B, Milbrandt J, Cavalli V, DiAntonio A (2012) Dual leucine zipper kinase is required for retrograde injury signaling and axonal regeneration. *Neuron* 74:1015–1022.
- Shin JE, Ha H, Kim YK, Cho Y, DiAntonio A (2019) DLK regulates a distinctive transcriptional regeneration program after peripheral nerve injury. *Neurobiol Dis* 127:178–192.
- Sigrist SJ, Thiel PR, Reiff DF, Lachance PED, Lasko P, Schuster CM (2000) Postsynaptic translation affects the efficacy and morphology of neuromuscular junctions. *Nature* 405:1062–1065.
- Skabkina OV, Skabkin MA, Popova NV, Lyabin DN, Penalva LO, Ovchinnikov LP (2003) Poly(A)-binding protein positively affects YB-1 mRNA translation through specific interaction with YB-1 mRNA. *J Biol Chem* 278:18191–18198.
- Sladic RT, Lagnado CA, Bagley CJ, Goodall GJ (2004) Human PABP binds AU-rich RNA via RNA-binding domains 3 and 4. *Eur J Biochem* 271:450–457.
- Smith RWP, Anderson RC, Larralde O, Smith JWS, Gorgoni B, Richardson WA, Malik P, Graham SV, Gray NK (2017) Viral and cellular mRNA-specific activators harness PABP and eIF4G to promote translation initiation downstream of cap binding. *Proc Natl Acad Sci U S A* 114:6310–6315.
- Srisawat C, Engelke DR (2001) Streptavidin aptamers: affinity tags for the study of RNAs and ribonucleoproteins. *RNA* 7:632–641.
- Sterne GR, Kim JH, Ye B (2015) Dysregulated Dscam levels act through Abelson tyrosine kinase to enlarge presynaptic arbors. *Elife* 4:e05196.
- Vazquez-Pianzola P, Urlaub H, Suter B (2011) Pabp binds to the osk 3'UTR and specifically contributes to osk mRNA stability and oocyte accumulation. *Dev Biol* 357:404–418.
- Wang X, Kim JH, Bazzi M, Robinson S, Collins CA, Ye B (2013) Bimodal control of dendritic and axonal growth by the dual leucine zipper kinase pathway. *PLoS Biol* 11:e1001572.
- Weidmann CA, Raynard NA, Blewett NH, Van Etten J, Goldstrohm AC (2014) The RNA binding domain of Pumilio antagonizes poly-adenosine binding protein and accelerates deadenylation. *Rna* 20:1298–1319.
- Wells SE, Hillner PE, Vale RD, Sachs AB (1998) Circularization of mRNA by eukaryotic translation initiation factors. *Mol Cell* 2:135–140.
- Wlaschin JJ, Gluski JM, Nguyen E, Silberberg H, Thompson JH, Chesler AT, Le Pichon CE (2018) Dual leucine zipper kinase is required for mechanical allodynia and microgliosis after nerve injury. *Elife* 7:e33910.
- Wu J, Bag J (1998) Negative control of the poly(A)-binding protein mRNA translation is mediated by the adenine-rich region of its 5'-untranslated region. *J Biol Chem* 273:34535–34542.
- Wu C, Wairkar YP, Collins CA, DiAntonio A (2005) Highwire function at the *Drosophila* neuromuscular junction: spatial, structural, and temporal requirements. *J Neurosci* 25:9557–9566.
- Xiong X, Wang X, Ewanek R, Bhat P, DiAntonio A, Collins CA (2010) Protein turnover of the Wallenda/DLK kinase regulates a retrograde response to axonal injury. *J Cell Biol* 191:211–223.
- Yan D, Wu Z, Chisholm AD, Jin Y (2009) The DLK-1 kinase promotes mRNA stability and local translation in *C. elegans* synapses and axon regeneration. *Cell* 138:1005–1018.
- Yang L, Li R, Kaneko T, Takle K, Morikawa RK, Essex L, Wang X, Zhou J, Emoto K, Xiang Y, Ye B (2014) Trim9 regulates activity-dependent fine-scale topography in *Drosophila*. *Curr Biol* 24:1024–1030.
- Zipursky SL, Sanes JR (2010) Chemoaffinity revisited: dscams, protocadherins, and neural circuit assembly. *Cell* 143:343–353.